PCCP

On the Linear Geometry of Lanthanide Hydroxide (Ln—OH, Ln=La-Lu)

Journal:	*Physical Chemistry Chemical Physics*
Manuscript ID	CP-ART-03-2019-001560.R2
Article Type:	Paper
Date Submitted by the Author:	02-Sep-2019
Complete List of Authors:	Harb, Hassan; University of California, Merced, Chemistry & Chemical Biology Thompson, Lee; University of Louisville, Department of Chemistry Hratchian, Hrant; University of California, Merced, Chemistry & Chemical Biology

On the Linear Geometry of Lanthanide Hydroxide (Ln—OH, Ln=La-Lu)

Hassan Harb, Lee M. Thompson,[†] and Hrant P. Hratchian[*],

Department of Chemistry & Chemical Biology and the Center for Chemical Computation and Theory, University of California, Merced, California 95343, USA

ABSTACT. Lanthanide hydroxides are key species in a variety of catalytic processes and in the preparation of corresponding oxides. This work explores the fundamental structure and bonding of the simplest lanthanide hydroxide, LnOH (Ln=La-Lu), using density functional theory calculations. Interestingly, the calculations predict that all structures of this series will be linear. Furthermore, these results indicate a valence electron configuration of $\sigma^2\pi^4$ for all LnOH compounds, suggesting that the lanthanide-hydroxide bond is best characterized as a covalent triple bond.

KEYWORDS. lanthanide, hydroxide, covalent bonding, d-orbitals, f-elements, bond theory

[†] Current address: Department of Chemistry, University of Louisville, Louisville, Kentucky 40292, USA.
[*] Email: hhratchian@ucmerced.edu

INTRODUCTION

Lanthanide compounds exhibit unique electronic and magnetic properties yielding a wide diversity of high-impact applications.[1-5] Lanthanides and, in particular, their corresponding hydrides, oxides, and hydroxides are known to efficiently facilitate important fundamental chemical transformations. Specific reactions catalyzed by such lanthanide species include oxidative dehydrogenation of alkenes, exchange of deuterium, and oxygen exchange.[1-14]

While the unique magnetic and optical properties of lanthanides have been attributed to partially filled 4f shells, it has been shown that these metal orbitals are essentially unaffected in ligand bonding and are, at most, weakly involved in chemical bonding. Indeed, their poor overlap with ligand orbitals results in very little energy stabilization.[15-17] Instead, bonding in such species is driven by 6s and 5d orbitals.[18] The question of covalent bonding in f element complexes has been an active research area for some time.[19-24] Work by B. Roos and P. Pyykkoo suggested lanthanide carbene ($LnCH_2^+$) compounds exhibit double bond character.[25] Bonding was found to involve 5d lanthanide orbitals while the 4f orbitals serve as spin counterweights and as an electron reservoir. Interestingly, studies on small actinide molecules have shown different bonding behavior, where, unlike lanthanides, 5f orbitals can significantly contribute to bonding. For instance, Kovacs has shown that AnO_3 exhibits actinide-oxygen bonds include contributions from actinide 5f orbitals.[26] Similar studies performed on AnC_2 and $AnCl_3$ have also implicated actinide 5f orbitals in bond formation.[26-32]

Motivated by our lab's recent interest in metal oxide clusters,[33-38] we were intrigued by an apparent dearth of literature exploring the structure and bonding of lanthanide hydroxides. With the goal of exploring the full series, we note the inclusion of PmOH; while included here for completeness, Pm is unstable and thus PmOH is not likely to be experimentally studied. Hydroxide

complexes play an important role in catalysis, biological systems, and in materials science.[4-5, 11] Thus, knowledge of bonding in such complexes will provide a more complete understanding of reaction mechanisms and enhance the development of new catalysts and new materials.[39] Of particular interest here is the series of LnOH complexes, which allows for the study of the fundamental aspects of hydroxide bonding with lanthanide metals. Furthermore, such cluster species serve as models for electronically strained defect sites on surfaces.[40] In support of this use of small molecules and clusters as models for such sites, Baker and coworkers recently demonstrated the highly localized nature of the electronic structure of metal oxides.[41]

In this study, density functional theory (DFT) is used to examine the electronic structure of lanthanide hydroxides. In particular, this report examines the ground state of each Ln—OH (Ln=La-Lu) followed by an in-depth investigation of the nature of the lanthanide-hydroxide bond. Relating this result to the well-studied structure and bonding of transition metal hydroxides,[42-50] we observe a similarity with early transition metal hydroxide bonding. Specifically, we show that the nature of the lanthanide hydroxide bond involves important π-bonding.

COMPUTATIONAL DETAILS

Calculations were carried out using a local development version of the Gaussian suite of electronic structure programs.[51] The B3PW91 density functional was employed[52-57] using the unrestricted spin formalism for open shell cases. The segmented all-electron relativistically contracted zeroth-order regular approximation (SARC-ZORA) basis set was used for all lanthanide centers.[58] This basis set provides an efficient alternative to effective core potentials in many routine DFT studies of similar species. Moreover, the SARC-ZORA basis set provides a balanced treatment of different electronic configurations of lanthanides.[58-60] The Dunning-style correlation

consistent basis set, aug-cc-pVTZ, was used for both hydrogen and oxygen centers.[61-62] To account for relativistic effects, the second-order Douglass-Kroll-Hess scalar relativistic correction was employed during geometry optimizations and frequency calculations.[63] Geometry optimizations were carried out using standard methods and all nature of all potential energy surface stationary points was confirmed by second-derivative calculations.[64] In all cases, the stability of converged Kohn-Sham determinants was verified.[65-66] Fragment-based orbital perturbation theory analysis was performed on all molecules using the Natural Bond Orbital program (NBO6).[67]

RESULTS AND DISCUSSIONS

To explore the structure and bonding of LnOH, we began by calculating minimum energy structures for each member of the series. Table 1 presents the geometric parameters of optimized LnOH structures. The lanthanide-oxygen bond lengths range from 1.90 to 2.09 Å and the O—H bond is consistently ~0.95Å through the series. For all species, the Ln–O–H bond angle is linear, suggesting two possible bonding descriptions. Either the compounds are covalently bound with the oxygen center adopting a sp hybridization and the Ln–OH bond featuring π-bonding character, or the system is best described as ionic and bound by a charge/dipole interaction. In an effort to fully characterize the Ln-hydroxide bond and understand the observed linear structure, three analyses have been carried out. Specifically, this study examines the canonical molecular orbitals (MOs) predicted by DFT, considers an analysis of ionic bond character, and employs a perturbational fragment MO analysis.[68-69]

Figure 1 shows the MO diagram of europium hydroxide, which is shown as a representative case for the LnOH series. The MO diagrams for the 14 other members of this series are substantially the same, with changes in the number of valence electrons resulting in a change

of electron count in 4f, 5d, and 6s based non-bonding orbitals. In addition to the differences in 4f occupations, GdOH and LuOH exhibit doubly-occupied 6s based non-bonding MOs. LaOH also has a doubly occupied 6s metal-based MO and an empty 4f manifold unlike the other LnOH species. The MO diagrams of CeOH, PrOH, NdOH, and PmOH share the common feature of a singly-occupied 5d orbital as the highest occupied MO (HOMO). Importantly, the relative energetic ordering of bonding and antibonding orbitals is unchanged across the full Ln series and, consequently, the Ln–(OH) bond order remains constant. Noteworthy are additional nearby low-energy states located for CeOH, NdOH, and PmOH. Indeed, multiple states for these species lie within a window of roughly 0.1 eV, which underscores how close-lying the 4*f*, 5*d* and 6*s* orbitals are in these molecules. In all cases, though, the minimum energy structure remains linear and the Ln–(OH) bond order is unchanged *(vide infra*). Full details regarding such states are provided in the Supporting Information.

Table 1. Optimized Geometries of Lanthanide Hydroxides.

Species	Ln—OH bond length (Å)	LnOH angle (degree)	O—H bond length (Å)
LaOH	2.04	180.0	0.96
CeOH	2.05	180.0	0.96
PrOH	2.05	180.0	0.95
NdOH	2.01	180.0	0.95
PmOH	2.03	180.0	0.95
SmOH	2.09	180.0	0.95
EuOH	2.08	180.0	0.95
GdOH	1.96	180.0	0.95
TbOH	2.01	180.0	0.95
DyOH	2.06	180.0	0.95
HoOH	2.05	180.0	0.95
ErOH	2.04	180.0	0.95
TmOH	2.03	180.0	0.95
YbOH	2.02	180.0	0.95
LuOH	1.90	180.0	0.95

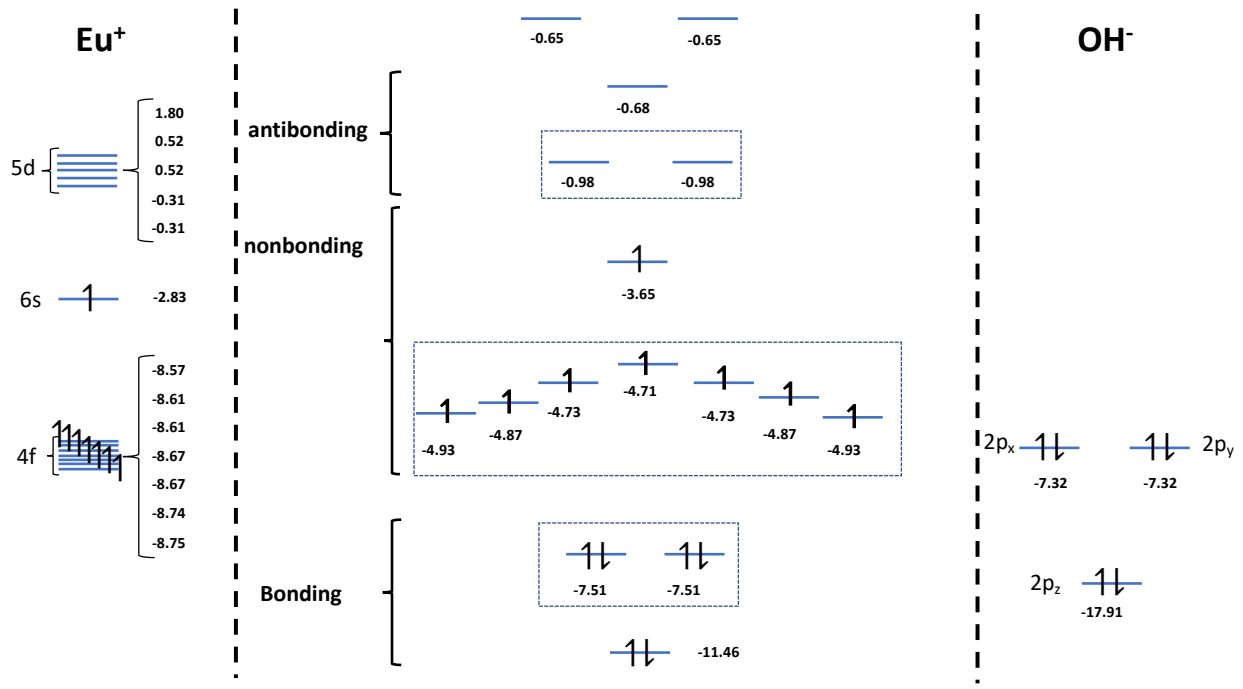

Figure 1. Orbital energies of the fragment Eu^+, OH^-, and the molecular orbital diagram of EuOH Orbital energies are given in eV.

Examination of the bonding orbitals supports assignment of the Ln—OH bond order as 3. Specifically, the MO diagram includes an occupied σ bonding orbital and two degenerate doubly-occupied π. The metal-based 4f and 6s orbitals are predominantly non-bonding. The 6s orbital is singly-occupied across the lanthanide hydroxide series except for LaOH, GdOH, and LuOH where the 6s based MO is doubly occupied as stated earlier, while 4f occupation changes with the atomic number of the lanthanide. A Mulliken population analysis (Supporting Information, Table S7) shows, as might be expected, that the bonding orbitals are mostly ligand based. Indeed, in both σ and π bonds the contribution from Ln centered atomic orbital basis functions can be as small as 3%. The Mulliken analysis further shows that metal participation in bonding primarily involves *p* and *d* Ln atomic orbitals, though the bonding in some members of the series includes some metal *f*-orbital character.

In order to explore the strength of the LnOH π MOs (Fig. 1), we investigated the dependence of the Ln—OH bond length with respect to changes in the Ln–O–H angle. Three specific LnOH cases were chosen: CeOH, EuOH, and YbOH. The bond lengths were relaxed while constraining the Ln–O–H angle to 109.5° and 120°. Table 2 shows the results of these calculations. For these three specific lanthanide hydroxides, the bond length decreases as the angle increases from 109° to the equilibrium value of 180°. This indicates that as the bond angle relaxes towards the linear minimum energy geometry, the sum of the covalent radii of the atoms decrease. Following Pyykko,[70-72] we interpret a decrease in the additive covalent radii as an indirect measure of an increase in bond order. Thus, the results of Table 2 indicate the bond order in the optimized linear structures is higher than in the bent structures.

Table 2. Variation in the bond length of some lanthanides at different Ln—O—H angles. Bond lengths are given in units of Angstroms.

Species	Ln—OH Bond Length at 109.5°	Ln—OH Bond Length at 120°	Ln—OH Bond length at 180°	%Difference from 109°	%Difference from 120°
CeOH	2.138	2.132	2.055	3.88	3.61
EuOH	2.153	2.143	2.084	3.20	2.75
YbOH	2.0746	2.0646	2.019	2.68	2.21

As mentioned above, the lanthanide-hydroxide linear geometry also could be due to electrostatic charge-dipole interactions. To explore this possibility, we compared optimized Ln—OH bond lengths with sums of Ln^+ and OH^- ionic radii.[73] An ideal ionic bond length is the sum of ionic radii of the two ions, and this value is expected to be appreciably larger than the associated covalent bond length. For the lanthanide ionic radii, where multiple radii are reported, we consider the smallest ionic radii for each lanthanide given by Shannon.[74] The reported ionic radii by

Shannon correspond to higher oxidation states (+2, +3, and +4) of the studied lanthanides. While the required Ln^+ and OH^- are missing, we can estimate their values by considering changes in ionic radii of ions as their oxidation states and coordination numbers change. A detailed description of the determination of the proper values of ionic radii for Ln^+ and OH^- is provided in the supporting information. Table 3 gives effective ionic radii and optimized bond lengths given by our DFT calculations for the LnOH series. In all cases, the optimized bond lengths are much shorter than the corresponding (ideal) LnOH ionic bond length. These results suggest Ln—OH bonding is not predominantly ionic in nature.

Table 3. Comparison of the ionic radii with the optimized bond lengths for Ln—OH. Distances are given in units of Angstroms.

Species	R(Ln+)	R(OH-)	R(Ln+) +R(OH-)	Bond Length	%Difference
LaOH	0.88	1.31	2.19	2.04	7.13
CeOH	0.86	1.31	2.17	2.05	5.78
PrOH	0.84	1.31	2.15	2.05	4.95
NdOH	0.84	1.31	2.15	2.01	6.74
PmOH	0.82	1.31	2.13	2.03	5.15
SmOH	0.81	1.31	2.12	2.09	1.64
EuOH	0.80	1.31	2.11	2.08	1.68
GdOH	0.79	1.31	2.10	1.96	7.39
TbOH	0.78	1.31	2.09	2.01	4.21
DyOH	0.78	1.31	2.09	2.06	1.22
HoOH	0.77	1.31	2.08	2.05	1.26
ErOH	0.76	1.31	2.07	2.04	1.30
TmOH	0.75	1.31	2.06	2.03	1.38
YbOH	0.74	1.31	2.05	2.02	1.38
LuOH	0.73	1.31	2.04	1.90	7.47

To more fully quantify the ionic character of the Ln-OH bond, we calculated the percent ionic character of the bond for each member in the series.[73] Specifically, dipole moments evaluated as part of our DFT calculations have been compared with dipoles evaluated classically between Ln cations and the hydroxide anion. For purely ionic systems, one would expect the ions to be Ln^{+} and OH^{-}.

Table 4. Comparison of the dipole moments of ideal ionic LnOH and optimized species. Dipoles are given in units of Debye.

Species	*Calculated Bond Length*	*Calculated Dipole Moment (DFT)*	*Idealized Dipole Moment (Placed at O)*	*Percent Ionic Character*
LaOH	2.04	0.04	9.76	0.4
CeOH	2.05	0.74	9.81	7.5
PrOH	2.05	0.87	9.77	8.9
NdOH	2.01	1.05	9.62	10.9
PmOH	2.03	1.15	9.68	11.9
SmOH	2.09	1.24	9.97	12.4
EuOH	2.08	1.42	9.95	14.3
GdOH	1.96	0.51	9.39	5.4
TbOH	2.01	0.60	9.61	6.2
DyOH	2.06	1.39	9.82	14.1
HoOH	2.05	1.52	9.79	15.5
ErOH	2.04	1.51	9.73	15.5
TmOH	2.03	1.60	9.69	16.5
YbOH	2.02	1.66	9.64	17.2
LuOH	1.9	0.47	9.05	5.2

As shown in Table 4, the ionic character of the Ln–(OH) bond varies with the lanthanide. For LaOH, which has zero f orbital population, the ionic character of the metal-hydroxide bond is essentially zero, suggesting the metal-hydroxide bond is purely covalent. The metal-hydroxide ionic bond character for the rest of the series varies from 5% at LuOH to 17% at YbOH. Stepping across the period from Ce to Eu, with a half-filled f shell, the ionic character of this bond increases. Another periodic trend of increasing ionic character is also observed as one moves across the series

from Gd to Yb. These trends may be understood by considering the occupation of f-based non-bonding MOs. In addition, the classical idealized dipole moment was calculated at two other cases (shown in Table 4). Specifically, in one case the center of the OH dipole fragment was taken to be at the midpoint of the O–H bond and in the other case the charge center was placed at the hydrogen nucleus. In both cases, the calculated dipole moment was larger than the dipole moment obtained from DFT calculations. The dipole moments resulting from these additional cases also resulted in a small percent ionic character (see Supporting Information).

To consider the extent of Ln–(OH) bond covalency, we performed a fragment based orbital perturbation study based on the Natural Bonding Orbital (NBO) model.[75] Specifically, the metal center (in the +1 oxidation state) and hydroxide ligand (–1 charge) were defined as separate fragments for the NBO fragment orbital second-order perturbation model. Table 5 reports NBO based second-order perturbation stabilization energies arising from inter-fragment occupied-unoccupied interactions.[67-69, 75] As seen in the MO diagram discussed above (Fig. 1), the LnOH series shows both σ and π bonding interactions. The NBO analysis (Fig. 2 and Table 5) supports this characterization. Indeed, the NBO study indicates that the σ bond is formed from hydroxide lone pair donation into the empty lanthanide $5d_{z2}$. In the second-order treatment of the model the stabilization energies from this bonding interaction are 11.2-25.4 kcal/mol. The NBO analysis also shows two significant interactions corresponding to π bonding between the lanthanides and hydroxide ligand. Such interactions result from lanthanide $5d_{xz}$ and $5d_{yz}$ orbitals interacting with hydroxide $2p_x$ and $2p_y$ orbitals. The calculated stabilization energies due to these π interactions range from 6.0 to 11.0 kcal/mol.

The σ and π stabilization energies increase with deceasing Ln—OH bond lengths (Table 1). However, rather than a single periodic trend being observed as one moves across the Ln series,

our results show bimodal behavior. Moving across the series from Ce to Eu, results in decreasing stabilization energies. A second decreasing trend begins at Gd and continues to Yb. Both La and Lu, the two extremes of the lanthanide series, are outliers. Similar to the discussion above regarding the ionic character of Ln–(OH) bonds, Ce-Eu/Gd-Yb trends can be understood by considering 6s5d4f occupations. Table 5 includes the known electron configurations for the lanthanide metals (in oxidation state I). The increase in f orbital occupation from Ce to Eu corresponds to the observed decrease in NBO stabilization energies for both σ and π bonds. Going from Eu to Gd, the increase in stabilization energies is due to occupation of the Gd 5d orbital, which is not common among the series (except for La and Ce). Stabilization energy decreases again to around 11 kcal/mol for the series Dy-Yb.

Table 5. Stabilization energies from Natural Bond Orbital analysis (NBO) along with the molecular term symbols and the orbital occupation of each species

Species	σ (Ln—OH) NBO stabilization energy (kcal/mol)	π (Ln—OH) NBO stabilization energies (kcal/mol)		Molecular Term Symbol	Orbital Occupation	Ln(I) electron configuration
LaOH	23.8	10.4	10.4	$^1\Sigma^+$	$4f^0\ 6s^2$	[Xe] $5d^2$
CeOH	18.3	9.3	9.3	^4H	$4f^1\ 6s^1\ 5d^1$	[Xe] $4f^1\ 5d^2$
PrOH	17.0	9.2	9.2	^5K	$4f^2\ 6s^1\ 5d^1$	[Xe] $4f^3\ 6s^1$
NdOH	18.2	10.2	8.7	^6L	$4f^3\ 6s^1\ 5d^1$	[Xe] $4f^4\ 6s^1$
PmOH	17.0	8.8	7.9	^7L	$4f^4\ 6s^1\ 5d^1$	[Xe] $4f^5\ 6s^1$
SmOH	14.6	6.6	6.6	$^8\Phi$	$4f^6\ 6s^1$	[Xe] $4f^6\ 6s^1$
EuOH	12.5	6.9	6.9	$^9\Sigma^-$	$4f^7\ 6s^1$	[Xe] $4f^7\ 6s^1$
GdOH	14.1	7.2	7.2	$^8\Sigma^-$	$4f^7\ 6s^2$	[Xe] $4f^7\ 5d^1\ 6s^1$
TbOH	14.2	7.6	7.3	^7K	$4f^9\ 6s^1$	[Xe] $4f^9\ 6s^1$
DyOH	11.7	6.4	6.3	^6I	$4f^{10}\ 6s^1$	[Xe] $4f^{10}\ 6s^1$
HoOH	11.6	6.2	6.2	^5I	$4f^{11}\ 6s^1$	[Xe] $4f^{11}\ 6s^1$
ErOH	11.2	6.0	6.0	^4H	$4f^{12}\ 6s^1$	[Xe] $4f^{12}\ 6s^1$
TmOH	11.2	6.1	5.8	$^3\Phi$	$4f^{13}\ 6s^1$	[Xe] $4f^{13}\ 6s^1$
YbOH	11.2	6.0	6.0	$^2\Sigma^-$	$4f^{14}\ 6s^1$	[Xe] $4f^{14}\ 6s^1$
LuOH	25.4	11.0	11.0	$^1\Sigma^-$	$4f^{14}\ 6s^2$	[Xe] $4f^{14}\ 6s^2$

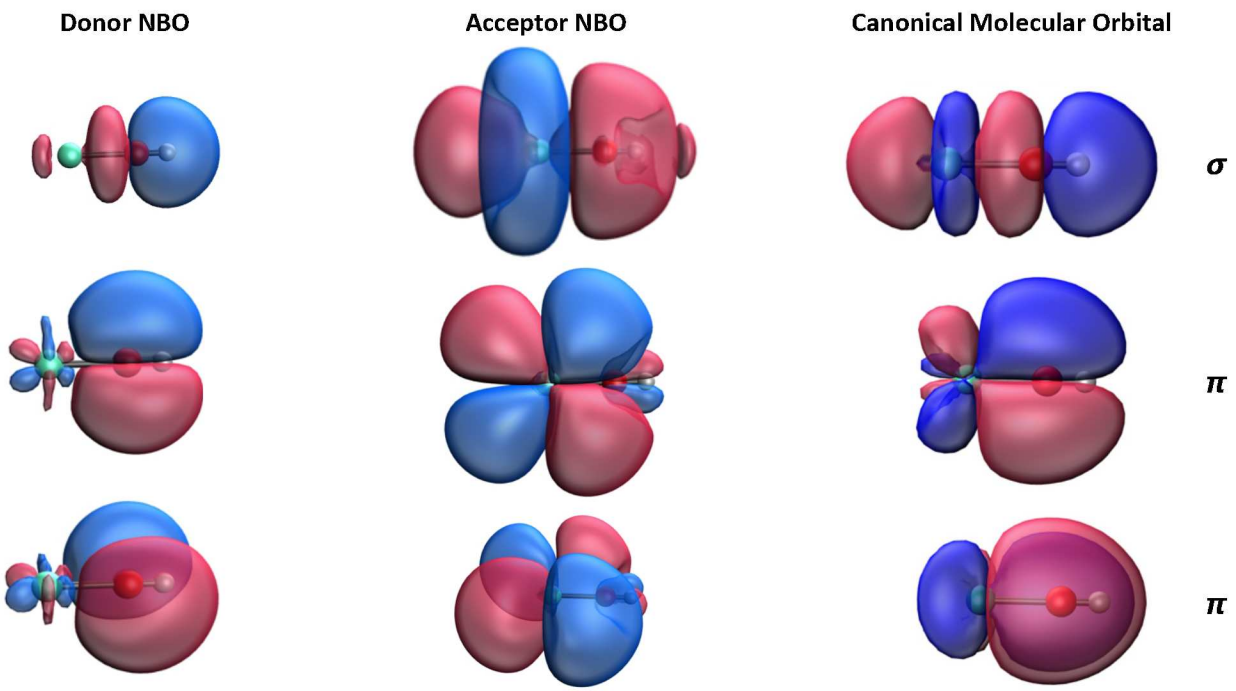

Figure 2. Natural Bond Orbitals of EuOH showing the donor and acceptor Natural Bond Orbitals (left and center columns) from metal(I) and OH^- fragments and corresponding resultant canonical molecular orbitals (right).

Linear metal-hydroxide compounds are not unique to the lanthanide species described in this work. Early first row transition metal hydroxides, ScOH, TiOH, and VOH, are also known to exhibit a linear conformation. Those systems feature σ bond donation from an oxygen lone pair to the empty metal $3d_{z2}$ orbital, as well as donation of two additional oxygen lone pairs to metal $3d_{xz}$ and $3d_{yz}$ orbitals. Thus, the bond order in those systems is 3,[42-44] just as our results suggest for LnOH.

Interestingly, the bonding changes as one moves from early to late transition metals. Various studies on CuOH report weaker Cu–OH bonding than for the early transition metals.[45-48] Previous studies, supported by both experimental and DFT calculations, have also shown that CuOH exhibits a bent geometry, unlike ScOH, TiOH or VOH.[46-47] For example, Karzhavyi et al.

reported a bent CuOH structure with a Cu—O—H angle of 107-110º in both a solid and a molecular calculation of CuOH.[48] Other previous work also suggest that zinc hydroxide exhibits a bent structure.[49-50] This difference in bonding trends between early and late transition metal hydroxides is due to differences in 5d occupation. As the d-orbital occupation increases, π-donation from the hydroxide lone pair orbitals becomes less favorable.

As mentioned, the LnOH species considered in this work have been motivated by recent fundamental bonding studies on gas phase lanthanide molecules and clusters. The analysis presented above suggests that in the case of multiple hydroxyl and oxo ligands coordination, one would expect a distortion of the Ln—O—H bond from its linear structure due to the inaccessibility of the lanthanide 5d orbitals. In recent studies, Chick Jarrold and coworkers presented the structure and bonding of various lanthanide oxides and hydroxides, some of which involve multiple lanthanide-oxygen bonds.[1, 14, 76-77] In agreement with our results, their experimental photoelectron spectroscopic studies and supporting DFT calculations have shown that Ln(I) complexes (e.g. $EuOH^1$) favor a linear geometry, while lanthanide complexes with a higher coordination number (two or more hydroxide ligands coordinated to the lanthanide center) and corresponding higher lanthanide oxidation state (+2, +3, etc.) yield bent Ln—O—H angles between 140º and 160º.[14, 77]

CONCLUSIONS

In this paper, DFT calculations have been used to explore the fundamental structure and bonding of lanthanide hydroxide complexes. For all members of this series, the minimum energy structure is a linear. An analysis of the canonical MOs establishes a metal-hydroxide bond order of 3, involving one σ- and two π- bonding MOs. Additional analysis suggests that the percent ionic character of the bond varies with the lanthanide metal. Interestingly, the degree of ionic character

is relatively small in all cases (ranging from < 1% to ~17%). A fragment based orbital perturbation study using the NBO model was employed to examine the strength of covalent bonding in the LnOH series. In agreement with the qualitative features of the canonical MOs, the NBO fragment orbital analysis identifies meaningful σ- and π-bonding interactions. Taken together, this work supports the assignment of the lanthanide-hydroxide bond as a triple bond.

ASSOCIATED CONTENT

Table providing total self-consistent energies, S^2 expectation values for all LnOH species discussed in the paper, descriptions of low-lying states located for select LnOH systems, and results from a Mulliken population analysis of the series of LnOH species.

ACKNOWLEDGMENT

We acknowledge financial support from UC Merced and computing time on the Multi-Environment Computer for Exploration and Discovery (MERCED) cluster which is supported by the National Science Foundation (Grant No. ACI-1429783). The donors of the American Chemical Society Petroleum Research Fund (ACS-PRF No. 56806-DNI6) are acknowledged for support of this work. HPH also thanks the Hellman Fellows Fund for a faculty fellowship.

REFERENCES

1. Kafader, J. O.; Ray, M.; Jarrold, C. C., Low-lying electronic structure of EuH, EuOH, and EuO neutrals and anions determined by anion photoelectron spectroscopy and DFT calculations. *J. Chem. Phys.* **2015,** *143* (3), 034305.
2. Mustachi, A., Mössbauer studies of europium and ytterbium hydrides. *J. Phys. Chem. Solids* **1974,** *35* (10), 1447-1450.
3. Ott, H.; Heise, S. J.; Sutarto, R.; Hu, Z.; Chang, C. F.; Hsieh, H. H.; Lin, H. J.; Chen, C. T.; Tjeng, L. H., Soft x-ray magnetic circular dichroism study on Gd-doped EuO thin films. *Phys. Rev. B* **2006,** *73* (9), 094407.
4. Schmehl, A.; Vaithyanathan, V.; Herrnberger, A.; Thiel, S.; Richter, C.; Liberati, M.; Heeg, T.; Rockerath, M.; Kourkoutis, L. F.; Muhlbauer, S.; Boni, P.; Muller, D. A.; Barash, Y.; Schubert, J.; Idzerda, Y.; Mannhart, J.; Schlom, D. G., Epitaxial integration of the highly spin-polarized ferromagnetic semiconductor EuO with silicon and GaN. *Nat. Mater.* **2007,** *6* (11), 882-887.
5. Swartz, A. G.; Ciraldo, J.; Wong, J. J. I.; Li, Y.; Han, W.; Lin, T.; Mack, S.; Shi, J.; Awschalom, D. D.; Kawakami, R. K., Epitaxial EuO thin films on GaAs. *Appl. Phys. Lett.* **2010,** *97* (11), 112509.
6. Infante, I.; Gagliardi, L.; Wang, X.; Andrews, L., Binding Motifs for Lanthanide Hydrides: A Combined Experimental and Theoretical Study of the $MH_x(H_2)_y$ Species (M = La−Gd; x = 1−4; y = 0−6). *J. Phys. Chem. A* **2009,** *113* (11), 2446-2455.
7. DiMarzio, D.; Croft, M.; Sakai, N.; Shafer, M. W., Effect of pressure on the electrical resistance of EuO. *Phys. Rev. B* **1987,** *35* (16), 8891-8893.
8. Shapira, Y.; Foner, S.; Reed, T. B., EuO. I. Resistivity and Hall Effect in Fields up to 150 kOe. *Phys. Rev. B* **1973,** *8* (5), 2299-2315.
9. Zanowick, R. L.; Wallace, W. E., Ferromagnetism in EuH_2. *Phys. Rev.* **1962,** *126* (2), 537-539.
10. Saitoh, H.; Machida, A.; Matsuoka, T.; Aoki, K., Phase diagram of the Eu–H system at high temperatures and high hydrogen pressures. *Solid State Commun.* **2015,** *205*, 24-27.
11. Souza-Neto, N. M.; Haskel, D.; Tseng, Y.-C.; Lapertot, G., Pressure-Induced Electronic Mixing and Enhancement of Ferromagnetic Ordering in EuX (X= Te, Se, S, O) Magnetic Semiconductors. *Phys. Rev. Lett.* **2009,** *102* (5), 057206.
12. Konno, T. J.; Ogawa, N.; Wakoh, K.; Sumiyama, K.; Suzuki, K., Synthesis and magnetic properties of non-equilibrium Eu-rich EuO thin films. *Jpn. J. Appl. Phys.* **1996,** *35* (12R), 6052.
13. Felton, J. A.; Ray, M.; Waller, S. E.; Kafader, J. O.; Jarrold, C. C., $Ce_xO_y^-$ (x = 2–3) + D_2O Reactions: Stoichiometric Cluster Formation from Deuteroxide Decomposition and Anti-Arrhenius Behavior. *J. Phys. Chem. A* **2014,** *118* (43), 9960-9969.
14. Topolski, J. E.; Kafader, J. O.; Ray, M.; Jarrold, C. C., Elucidating cerium + H_2O reactivity through electronic structure: A combined PES and DFT study. *J. Mol. Spectrosc.* **2017,** *336*, 1-11.
15. Axe, J.-D.; Burns, G., Influence of covalency upon rare-earth ligand field splittings. *Phys. Rev.* **1966,** *152* (1), 331.
16. Bursten, B.; Palmer, E.; Sonnenberg, J., On the Role of f-Obitals in the Bonding in f-Element Complexes. *Spec. Publ. - R. Soc. Chem.* **2006,** *305* (1), 157-162.
17. Minasian, S. G.; Batista, E. R.; Booth, C. H.; Clark, D. L.; Keith, J. M.; Kozimor, S. A.; Lukens, W. W.; Martin, R. L.; Shuh, D. K.; Stieber, S. C. E., Quantitative evidence for lanthanide-oxygen orbital mixing in CeO_2, PrO_2, and TbO_2. *J. Am. Chem. Soc.* **2017,** *139* (49), 18052-18064.

18. Maron, L.; Eisenstein, O., Do f Electrons Play a Role in the Lanthanide− Ligand Bonds? A DFT Study of Ln $(NR_2)_3$; R= H, SiH_3. *J. Phys. Chem. A* **2000,** *104* (30), 7140-7143.
19. Barros, N.; Maynau, D.; Maron, L.; Eisenstein, O.; Zi, G.; Andersen, R. A., Single but stronger UO, double but weaker UNMe bonds: the tale told by Cp_2UO and Cp_2UNR. *Organometallics* **2007,** *26* (20), 5059-5065.
20. Kaltsoyannis, N., Does covalency increase or decrease across the actinide series? Implications for minor actinide partitioning. *Inorg. Chem.* **2012,** *52* (7), 3407-3413.
21. Kelley, M. P.; Su, J.; Urban, M.; Luckey, M.; Batista, E. R.; Yang, P.; Shafer, J. C., On the Origin of Covalent Bonding in Heavy Actinides. *J. Am. Chem. Soc.* **2017**.
22. Lukens, W. W.; Edelstein, N. M.; Magnani, N.; Hayton, T. W.; Fortier, S.; Seaman, L. A., Quantifying the σ and π interactions between U (V) f orbitals and halide, alkyl, alkoxide, amide and ketimide ligands. *J. Am. Chem. Soc.* **2013,** *135* (29), 10742-10754.
23. Neidig, M. L.; Clark, D. L.; Martin, R. L., Covalency in f-element complexes. *Coordination Chem. Rev.* **2013,** *257* (2), 394-406.
24. Dognon, J. P.; Pyykkö, P., Chemistry of the 5g Elements: Relativistic Calculations on Hexafluorides. *Angew. Chem., Int. Ed.* **2017**.
25. Roos, B. O.; Pyykkö, P., Bonding Trends in Molecular Compounds of Lanthanides: The Double-Bonded Carbene Cations $LnCH_2^+$ (Ln= Sc, Y, La–Lu). *Chem. - Eur. J.* **2010,** *16* (1), 270-275.
26. Kovács, A., Relativistic Multireference Quantum Chemical Study of the Electronic Structure of Actinide Trioxide Molecules. *J. Phys. Chem. A* **2017,** *121* (12), 2523-2530.
27. Pyykkö, P., Additive covalent radii for single-, double-, and triple-bonded molecules and tetrahedrally bonded crystals: a summary. *J. Phys. Chem. A* **2014,** *119* (11), 2326-2337.
28. Kovács, A.; Konings, R. J. M., Computed Vibrational Frequencies of Actinide Oxides $AnO^{0/+/2+}$ and $AnO_2^{0/+/2+}$(An= Th, Pa, U, Np, Pu, Am, Cm). *J. Phys. Chem. A* **2011,** *115* (24), 6646-6656.
29. Kovács, A.; Konings, R. J. M.; Varga, Z. n.; Szieberth, D. n., Structure and Other Molecular Properties of Actinide Trichlorides $AnCl_3$ (An= Th–Cm). *J. Phys. Chem. A* **2013,** *117* (44), 11357-11363.
30. Hratchian, H. P.; Sonnenberg, J. L.; Hay, P. J.; Martin, R. L.; Bursten, B. E.; Schlegel, H. B., Theoretical investigation of uranyl dihydroxide: oxo ligand exchange, water catalysis, and vibrational spectra. *J. Phys. Chem. A* **2005,** *109* (38), 8579-8586.
31. Sonnenberg, J. L.; Hay, P. J.; Martin, R. L.; Bursten, B. E., Theoretical Investigations of Uranyl–Ligand Bonding: Four-and Five-Coordinate Uranyl Cyanide, Isocyanide, Carbonyl, and Hydroxide Complexes. *Inorg. Chem.* **2005,** *44* (7), 2255-2262.
32. Pogány, P.; Kovács, A.; Varga, Z.; Bickelhaupt, F. M.; Konings, R. J. M., Theoretical Study of the Structure and Bonding in ThC_2 and UC_2. *J. Phys. Chem. A* **2011,** *116* (1), 747-755.
33. Thompson, L. M.; Jarrold, C. C.; Hratchian, H. P., Explaining the $MoVO_4^-$ photoelectron spectrum: Rationalization of geometric and electronic structure. *J. Chem. Phys.* **2017,** *146* (10), 104301.
34. Thompson, L. M.; Hratchian, H. P., Modeling the Photoelectron Spectra of $MoNbO_2^-$ Accounting for Spin Contamination in Density Functional Theory. *J. Phys. Chem. A* **2015,** *119* (32), 8744-8751.
35. Mason, J. L.; Harb, H.; Topolski, J. E.; Hratchian, H. P.; Jarrold, C. C., A Tale of Two Stabilities: How One Boron Atom Affects a Switch in Bonding Motifs in $CeO_2B_x^-$ (x = 2, 3) Complexes. *J. Phys. Chem. A* **2018,** *122* (51), 9879-9885.

36. Topolski, J. E.; Kafader, J. O.; Marrero-Colon, V.; Iyengar, S. S.; Hratchian, H. P.; Jarrold, C. C., Exotic electronic structures of $Sm_xCe_{3-x}O_y$ (x = 0-3; y = 2-4) clusters and the effect of high neutral density of low-lying states on photodetachment transition intensities. *J. Chem. Phys.* **2018,** *149* (5), 054305.
37. Mason, J. L.; Harb, H.; Huizenga, C. D.; Ewigleben, J. C.; Topolski, J. E.; Hratchian, H. P.; Jarrold, C. C., Electronic and Molecular Structures of the CeB_6 Monomer. *J. Phys. Chem. A* **2019,** *123* (10), 2040-2048.
38. DeVine, J. A.; Abou Taka, A.; Babin, M. C.; Weichman, M. L.; Hratchian, H. P.; Neumark, D. M., High-resolution photoelectron spectroscopy of $TiO_3H_2^-$: Probing the TiO_2^- + H_2O dissociative adduct. *J. Chem. Phys.* **2018,** *148* (22), 222810.
39. Zhang, X.; Schwarz, H., Bonding in cationic MOH_n^+ (M= K− La, Hf− Rn; n= 0–2): DFT performances and periodic trends. *Theor. Chem. Acc.* **2011,** *129* (3-5), 389-399.
40. Mann, J. E.; Mayhall, N. J.; Jarrold, C. C., Properties of metal oxide clusters in non-traditional oxidation states. *Chem. Phys. Lett.* **2012,** *525*, 1-12.
41. Biswas, S.; Husek, J.; Londo, S.; Baker, L. R., Highly Localized Charge Transfer Excitons in Metal Oxide Semiconductors. *Nano Lett.* **2018,** *18* (2), 1228-1233.
42. Miliordos, E.; Hunt, K. L., First-Principles Calculations of the Electronic and Geometrical Structures of Neutral [Sc, O, H] Molecules and the Monocations, $ScOH^{0,+}$ and $HScO^{0,+}$. *J. Phys. Chem. A* **2011,** *115* (17), 4436-4447.
43. Miliordos, E.; Harrison, J. F.; Hunt, K. L., Ab initio investigation of titanium hydroxide isomers and their cations, $TiOH^{0,+}$ and $HTiO^{0,+}$. *J. Chem. Phys.* **2011,** *135* (14), 144111.
44. Miliordos, E.; Harrison, J. F.; Hunt, K. L., Ground and excited states of vanadium hydroxide isomers and their cations, $VOH^{0,+}$ and $HVO^{0,+}$. *J. Chem. Phys.* **2013,** *138* (11), 114305.
45. Rezabal, E.; Ruipérez, F.; Ugalde, J., Quantum chemical study of the catalytic activation of methane by copper oxide and copper hydroxide cations. *Phys. Chem. Chem. Phys.* **2013,** *15* (4), 1148-1153.
46. Soroka, I. L.; Shchukarev, A.; Jonsson, M.; Tarakina, N. V.; Korzhavyi, P. A., Cuprous hydroxide in a solid form: does it exist? *Dalton Trans.* **2013,** *42* (26), 9585-9594.
47. Li, Y.; Lousada, C. u. M.; Soroka, I. L.; Korzhavyi, P. A., Bond network topology and antiferroelectric order in cuprice CuOH. *Inorg. Chem.* **2015,** *54* (18), 8969-8977.
48. Korzhavyi, P. A.; Soroka, I. L.; Isaev, E. I.; Lilja, C.; Johansson, B., Exploring monovalent copper compounds with oxygen and hydrogen. *Proc. Natl. Acad. Sci. U.S.A.* **2012,** *109* (3), 686-689.
49. Stählin, W.; Oswald, H. R., The crystal structure of zinc hydroxide nitrate, $Zn_5(OH)_8(NO_3)_2.2H_2O$. *Acta Crystallogr., Sect. B: Struct. Crystallogr. Cryst. Chem.* **1970,** *26* (6), 860-863.
50. Arizaga, G. G. C.; Satyanarayana, K. G.; Wypych, F., Layered hydroxide salts: synthesis, properties and potential applications. *Solid State Ionics* **2007,** *178* (15), 1143-1162.
51. Frisch, M. J.; H. B. Schlegel, G. E. S., M. A. Robb, J. R. Cheeseman, G. Scalmani, V. Barone, B. Mennucci, G. A. Petersson, H. Nakatsuji, M. Caricato, X. Li, H. P. Hratchian, A. F. Izmaylov, J. Bloino, B. Janesko, F. Lipparini, G. Zheng, J. L. Sonnenberg, W. Liang, M. Hada, M. Ehara, K. Toyota, R. Fukuda, J. Hasegawa, M. Ishida, T. Nakajima, Y. Honda, O. Kitao, H. Nakai, T. Vreven, J. A. Montgomery, Jr., J. E. Peralta, F. Ogliaro, M. Bearpark, J. J. Heyd, E. Brothers, K. N. Kudin, V. N. Staroverov, T. Keith, R. Kobayashi, J. Normand, K. Raghavachari, A. Rendell, J. C. Burant, S. S. Iyengar, J. Tomasi, M. Cossi, N. Rega, J. M. Millam, M. Klene, J. E. Knox, J. B. Cross, V. Bakken, C. Adamo, J. Jaramillo, R. Gomperts, R. E. Stratmann, O. Yazyev, A. J. Austin,

R. Cammi, C. Pomelli, J. W. Ochterski, R. L. Martin, K. Morokuma, V. G. Zakrzewski, G. A. Voth, P. Salvador, J. J. Dannenberg, S. Dapprich, P. V. Parandekar, N. J. Mayhall, A. D. Daniels, O. Farkas, J. B. Foresman, J. V. Ortiz, J. Cioslowski, and D. J. Fox, Gaussian Development Version, Revision I.03+, Gaussian, Inc., Wallingford CT,. **2018**.

52. Perdew, J. P.; Chevary, J. A.; Vosko, S. H.; Jackson, K. A.; Pederson, M. R.; Singh, D. J.; Fiolhais, C., Atoms, molecules, solids, and surfaces: Applications of the generalized gradient approximation for exchange and correlation. *Physical Review B* **1992,** *46* (11), 6671-6687.
53. Perdew, J. P.; Wang, Y., Accurate and simple analytic representation of the electron-gas correlation energy. *Phys. Rev. B* **1992,** *45* (23), 13244-13249.
54. Becke, A. D., Density-functional thermochemistry. IV. A new dynamical correlation functional and implications for exact-exchange mixing. *J. Chem. Phys.* **1996,** *104* (3), 1040-1046.
55. Becke, A. D., Density-functional thermochemistry. III. The role of exact exchange. *J. Chem. Phys.* **1993,** *98* (7), 5648-5652.
56. Becke, A. D., Density-functional thermochemistry. II. The effect of the Perdew–Wang generalized-gradient correlation correction. *J. Chem. Phys.* **1992,** *97* (12), 9173-9177.
57. Becke, A. D., Density-functional thermochemistry. I. The effect of the exchange-only gradient correction. *J. Chem. Phys.* **1992,** *96* (3), 2155-2160.
58. Pantazis, D. A.; Neese, F., All-electron scalar relativistic basis sets for the lanthanides. *J. Chem. Theory Comput.* **2009,** *5* (9), 2229-2238.
59. Pantazis, D. A.; Neese, F., All-electron scalar relativistic basis sets for the 6p elements. *Theor. Chem. Acc.* **2012,** *131* (11), 1-7.
60. Dolg, M., Segmented contracted Douglas–Kroll–Hess adapted basis sets for lanthanides. *J. Chem. Theory Comput.* **2011,** *7* (10), 3131-3142.
61. Kendall, R. A.; Jr., T. H. D.; Harrison, R. J., Electron affinities of the first-row atoms revisited. Systematic basis sets and wave functions. *J. Chem. Phys.* **1992,** *96* (9), 6796-6806.
62. Papajak, E.; Zheng, J.; Xu, X.; Leverentz, H. R.; Truhlar, D. G., Perspectives on Basis Sets Beautiful: Seasonal Plantings of Diffuse Basis Functions. *J. Chem. Theory Comput.* **2011,** *7* (10), 3027-3034.
63. Nakajima, T.; Hirao, K., The Douglas–Kroll–Hess Approach. *Chem. Rev.* **2011,** *112* (1), 385-402.
64. Hratchian, H. P.; Schlegel, H. B., Finding Minima, Transition States, and Following Reaction Pathways on Ab Initio Potential Energy Surfaces. In *Theory and Applications of Computational Chemistry: The First Forty Years*, Dykstra, C. E.; Frenking, G.; Kim, K. S.; Scuseria, G. E., Eds. Elsevier: Amsterdam, 2005; p 195.
65. Bauernschmitt, R.; Ahlrichs, R., Stability analysis for solutions of the closed shell Kohn–Sham equation. *J. Chem. Phys.* **1996,** *104* (22), 9047-9052.
66. Seeger, R.; Pople, J. A., Self-consistent molecular orbital methods. XVIII. Constraints and stability in Hartree–Fock theory. *J. Chem. Phys.* **1977,** *66* (7), 3045-3050.
67. Glendening, E. D.; Badenhoop, J. K.; Reed, A. E.; Carpenter, J. E.; Bohmann, J. A.; Morales, C. M.; Landis, C. R.; Weinhold, F., Natural bond orbital analysis program: NBO 6.0. *Theoretical Chemistry Institute, University of Wisconsin, Madison, WI* **2013**.
68. Foster, J. P.; Weinhold, F., Natural hybrid orbitals. *J. Am. Chem. Soc.* **1980,** *102* (24), 7211-7218.
69. Reed, A. E.; Weinhold, F., Natural bond orbital analysis of near-Hartree–Fock water dimer. *J. Chem. Phys.* **1983,** *78* (6), 4066-4073.

70. Pyykkö, P.; Atsumi, M., Molecular Double-Bond Covalent Radii for Elements Li–E112. *Chem. - Eur. J.* **2009,** *15* (46), 12770-12779.
71. Pyykkö, P.; Atsumi, M., Molecular Single-Bond Covalent Radii for Elements 1–118. *Chem. - Eur. J.* **2009,** *15* (1), 186-197.
72. Pyykkö, P.; Riedel, S.; Patzschke, M., Triple-Bond Covalent Radii. *Chem. - Eur. J.* **2005,** *11* (12), 3511-3520.
73. Pauling, L., *General Chemistry*. Courier Corporation: 1988.
74. Shannon, R. D., Revised effective ionic radii and systematic studies of interatomic distances in halides and chalcogenides. *Acta Crystallogr., Sect. A: Cryst. Phys., Diffr., Theor. Gen. Crystallogr.* **1976,** *32* (5), 751-767.
75. Weinhold, F., Natural bond orbital analysis: A critical overview of relationships to alternative bonding perspectives. *J. Comput. Chem.* **2012,** *33* (30), 2363-2379.
76. Ray, M.; Felton, J. A.; Kafader, J. O.; Topolski, J. E.; Jarrold, C. C., Photoelectron spectra of CeO^- and $Ce(OH)_2^-$. *J. Chem. Phys.* **2015,** *142* (6), 064305.
77. Topolski, J. E.; Kafader, J. O.; Jarrold, C. C., Ce in the +4 oxidation state: Anion photoelectron spectroscopy and photodissociation of small $Ce_xO_yH_z^-$ molecules. *J. Chem. Phys.* **2017,** *147* (10), 104303.

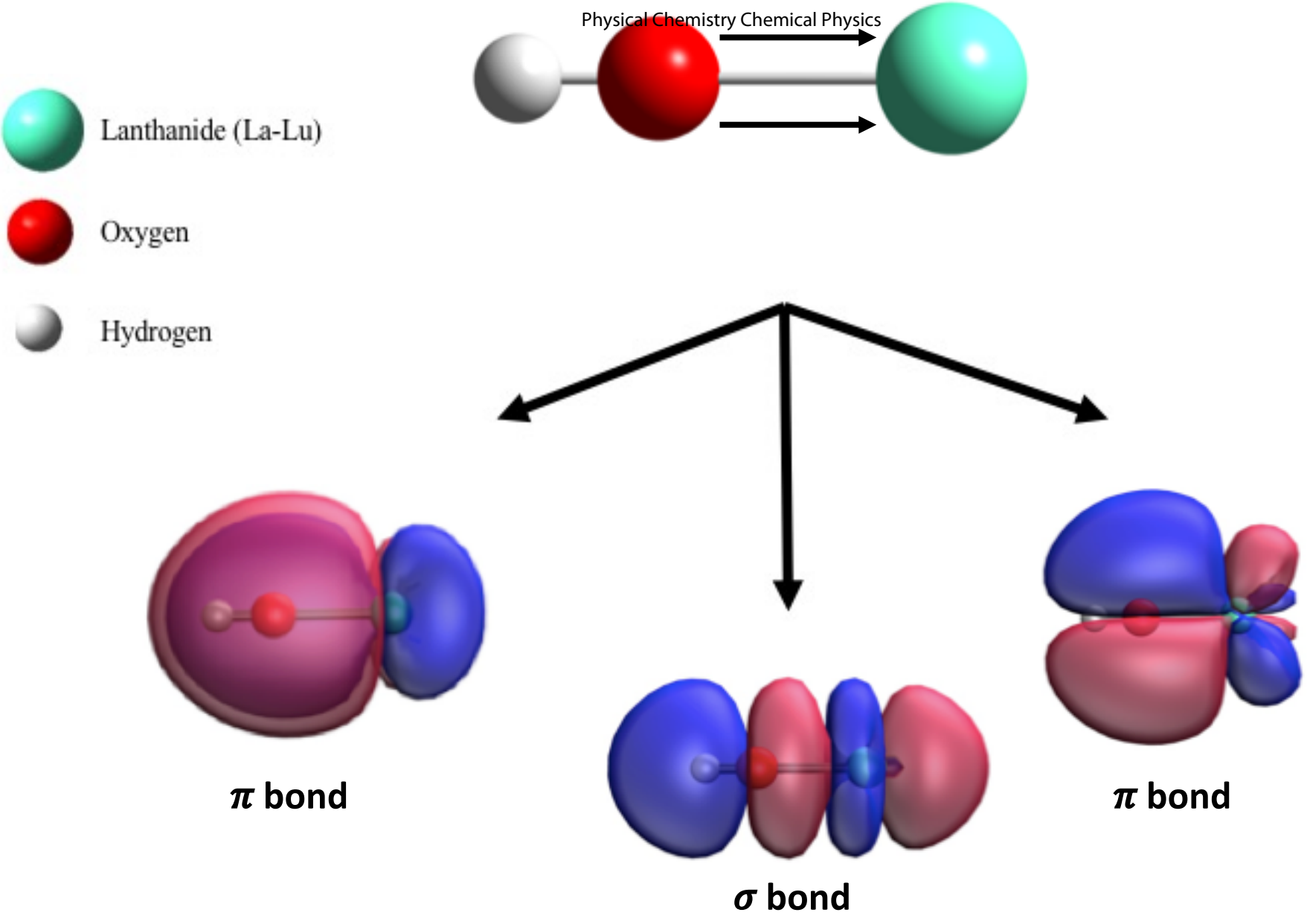
Lanthanide (La-Lu)
Oxygen
Hydrogen
π bond
σ bond
π bond